Curved Planar Reformatting and Convolutional Neural Network-Based Segmentation of the Small Bowel for Visualization and Quantitative Assessment of Pediatric Crohn's Disease From MRI

Yechiel Lamash, PhD,[1]* Sila Kurugol, PhD,[1] Moti Freiman, PhD,[1] Jeannette M. Perez-Rossello, MD,[2] Michael J. Callahan, MD,[2] Athos Bousvaros, MD, MPH,[3] and Simon K. Warfield, PhD[1]

Background: Contrast-enhanced MRI of the small bowel is an effective imaging sequence for the detection and characterization of disease burden in pediatric Crohn's disease (CD). However, visualization and quantification of disease burden requires scrolling back and forth through 3D images to follow the anatomy of the bowel, and it can be difficult to fully appreciate the extent of disease.
Purpose: To develop and evaluate a method that offers better visualization and quantitative assessment of CD from MRI.
Study Type: Retrospective.
Population: Twenty-three pediatric patients with CD.
Field Strength/Sequence: 1.5T MRI system and T_1-weighted postcontrast VIBE sequence.
Assessment: The convolutional neural network (CNN) segmentation of the bowel's lumen, wall, and background was compared with manual boundary delineation. We assessed the reproducibility and the capability of the extracted markers to differentiate between different levels of disease defined after a consensus review by two experienced radiologists.
Statistical Tests: The segmentation algorithm was assessed using the Dice similarity coefficient (DSC) and boundary distances between the CNN and manual boundary delineations. The capability of the extracted markers to differentiate between different disease levels was determined using a *t*-test. The reproducibility of the extracted markers was assessed using the mean relative difference (MRD), Pearson correlation, and Bland–Altman analysis.
Results: Our CNN exhibited DSCs of 75 ± 18%, 81 ± 8%, and 97 ± 2% for the lumen, wall, and background, respectively. The extracted markers of wall thickness at the location of min radius ($P = 0.0013$) and the median value of relative contrast enhancement ($P = 0.0033$) could differentiate active and nonactive disease segments. Other extracted markers could differentiate between segments with strictures and segments without strictures ($P < 0.05$). The observers' agreement in measuring stricture length was >3 times superior when computed on curved planar reformatting images compared with the conventional scheme.
Data Conclusion: The results of this study show that the newly developed method is efficient for visualization and assessment of CD.
Level of Evidence: 4
Technical Efficacy: Stage 2

J. MAGN. RESON. IMAGING 2018.

View this article online at wileyonlinelibrary.com. DOI: 10.1002/jmri.26330

Received Jun 1, 2018, Accepted for publication Aug 20, 2018.

*Address reprint requests to: Y.L., Computational Radiology Laboratory, Dept. of Radiology, Children's Hospital Boston, Harvard Medical School, 300 Longwood Ave., Boston MA, 02115. E-mail: shilikster@gmail.com

From the [1]Computational Radiology Laboratory, Department of Radiology, Children's Hospital Boston, Harvard Medical School, Boston, Massachusetts, USA; [2]Department of Radiology, Children's Hospital Boston, Harvard Medical School, Boston, Massachusetts, USA; and [3]Center for Inflammatory Bowel Disease Treatment and Research, Children's Hospital Boston, Harvard Medical School, Boston, Massachusetts, USA

Magnetic resonance enterography (MRE) has emerged as an effective method for imaging the small bowel in patients with Crohn's disease (CD).[1] MRE is especially useful for pediatric CD patients as we strive to spare children the potentially harmful effects of radiation. Information conveying length of involvement, severity of inflammation, and luminal narrowing are required when assessing medical therapeutic response or decision for surgical treatment.[1,2] To facilitate these measurements, several computational methods have been proposed.[3–11] However, to date there is not a single segmentation method that extracts the tubular structure of the diseased small bowel and includes both the lumen and wall compartments. Such segmentation is essential, as it is the only way to enable the analysis of wall thickness, tissue enhancement, and lumen narrowing along the diseased segment.

Curved planar reformatting (CPR) views are commonly used by radiologists and clinicians to demonstrate pathology in curved organs such as blood vessels, the spine, and the colon.[12] This technique is a key enabler in many clinical applications, giving the ability to visualize and assess luminal narrowing and serve as a platform for segmentation and editing. CPR views provide comprehensive and clear depiction of the disease state on a single image. Such images can be saved as a bookmark, shared among clinicians and used for evaluating change during therapy. However, despite the common use of CPR views in these curved organs, there seem to be no easily mastered tools for analyzing magnetic resonance imaging (MRI) of the small bowel. As a result, the radiologist or clinician is constrained to scrolling back and forth through 2D images in order to understand the 3D structure of the abnormality.

Another limitation is the lack of labeled datasets required for training sophisticated supervised machine-learning algorithms. Deep-learning algorithms, in particular, convolutional neural networks (CNNs), have rapidly become a methodology of choice for analyzing medical images.[13] Thanks to its unique capability of learning hierarchical feature representations solely from data, deep learning has achieved record-breaking performance in a variety of artificial intelligence applications and grand challenges.[14] In addition, the runtime of trained networks on new data is very fast (typically on the order of seconds). Such networks generally have a large number of parameters and training them requires a correspondingly large dataset. However, there are not enough publicly available labeled datasets and it is labor-intensive to manually label images for segmentation. Specifically, for our problem, there is no publicly available training data.

The purpose of the current preliminary study is to develop and evaluate the feasibility of a new 3D processing technique for improving the visualization and extraction of CD quantitative imaging markers from MRI.

Materials and Methods

We developed a software tool that generates CPR images and provide editing tools that can be used for several purposes: first, it enables visualization and measurement of degree and length of luminal stenosis; second, it can be used for generation of annotated dataset to train supervised bowel wall segmentation algorithms; third, it serves as a platform providing efficient editing tools for refinement of the automatic wall segmentation results if needed; finally, it provides a comprehensive depiction of disease severity in a single image. After generating annotated dataset of the small bowel lumen and wall, we trained a fully convolutional neural network architecture[15] with residual units[16] and a distance channel prior for segmenting the small bowel lumen and wall. Although the results of the automatic segmentation are quite satisfactory, we can refine the resultant segmentations using the proposed editing tools when needed.

Generating CPR Views for the Small Bowel

CPR view generation starts with placement of seed points along the lumen's centerline. We have generated practical and stable visualization software implemented in MatLab (MathWorks, Natick, MA) to achieve that goal. Our software visualizes coronal, sagittal, and axial views that are automatically synchronized to the user's curser location. This enables the user to position seed points in the most visible cross-section along the curved lumen. If the lumen is completely obstructed, we select seed points in the middle of the obstruction. Before the analysis, we interpolated the image volumes to isotropic sampling resolution.

Given a set of points on the centerline curve, we perform arclength parameterization[17] to obtain an equally sampled curve. We first interpolate between the seed points to get a curve $\vec{r}(t) = [X(t), Y(t), Z(t)]$.

We then perform integral to get the arclength parameter s as a function of t:

$$s(t) = \int_0^t \|\vec{r}(t)\| dt$$

Since s is monotonic, we can calculate its inverse function along s:

$$t(s) = \underset{t}{\operatorname{argmin}} |s(t) - s|$$

Finally, we interpolate the curve along s:

$$r(s) = [X(t(s)), Y(t(s)), Z(t(s))]$$

Generating a stretched CPR view include the following stages: 1) select a plane transverse through the two extreme points and another interactively selected third point; 2) project the curve onto that plane[12]; 3) perform arclength parameterization to the projected curve; 4) interpolate the stretched CPR image by traversing on the projected curve at equal speed where each row is a ray perpendicular to the projected curve.

For straightened CPR view, we set the Frenet-Serret frame[18] along the curve and interpolate images on the planes normal to the curve. Given a curve with arclength parameterization, the Frenet-Serret equations are given by:

$$\vec{T}(s) = dr/ds/\|dr/ds\|$$
$$\vec{N}(s) = dT/ds/\|dT/ds\|$$
$$\vec{B}(s) = \vec{B}(s) \times \vec{T}(s)$$

where, T, N, and B are the tangent, principle normal, and secondary normal vectors, respectively.

Before calculating the Frenet-Serret frame vectors, we used the Savitzky-Golay[19] filtering to smooth the centerline curve and the orthogonal vectors along it.

In order to prevent discontinuities in the straightened CPR views that may occur due to locations with sharp curvature, we find the angle between adjacent normal vectors along the curve and rotate the normal vectors to align with the normal vector at $s = 0$.

In order to do so, we project each normal vector at location $s-1$ on the normal plane at location s and calculate the projected normal angle with respect to the normal plane vectors $\vec{N}_s$, $\vec{B}_s$:

$$d\theta(s) = \tan^{-1}(\langle \vec{N}_{s-1}, \vec{N}_s \rangle / \langle \vec{N}_{s-1}, \vec{B}_s \rangle)$$

Then the global required angle of the normal vector at position s is obtained by:

$$\theta(s) = \int_0^s d\theta ds$$

We then calculate new normal plane vectors $\vec{N}_n(s), \vec{B}_n(s)$ by rotating them on the normal plane with angleθ. We define a [3x3] matrix A:

$$A = \begin{bmatrix} \vec{N}^T(s) \\ \vec{B}^T(s) \\ \vec{T}^T(s) \end{bmatrix}$$

And calculate the new normal plane vectors as follows:

$$\vec{N}_n(s) = A^{-1} \cdot \begin{bmatrix} \cos(\theta) \\ \sin(\theta) \\ 0 \end{bmatrix}$$

$$\vec{B}_n(s) = \vec{T}(s) \times \vec{N}_n(s)$$

Figure 1 demonstrates several results of stretched and straightened CPR views of small bowel segments with CD from contrast-enhanced T_1-weighted MR images that contain regions with strictures (narrowing).

Bowel Lumen and Wall Segmentation

GENERATION OF ANNOTATED DATASET. The generation of high-quality annotated datasets is an essential component for training an accurate supervised segmentation algorithm. In order to generate an annotated dataset in a reasonable amount of time, we started with automatic segmentation and then refined the results. We therefore performed the following stages: first, we used graph cut segmentation[20] to obtain an initial segmentation of the bowel wall boundaries. Next, we manually refined the segmentation contours on six straightened CPR images. Then we generate a tetrahedral mesh to transfer the segmentation represented by the contours in the straightened CPR views into a volumetric representation. Finally, we refined the volumetric annotations in the original acquisition planes.

INITIAL GRAPH CUT SEGMENTATION. Due to the axially symmetric representation of the bowel in the straightened CPR volume (eg, Fig. 1d,e), we set the connectivity of the graph to be between pixels represented in cylindrical coordinates. We therefore sampled straightened CPR images every 5 degrees to generate a volume in which each image represents a slice that passes through the center at a specific angleθ. Using this representation, we segment the volume into five layers (or classes) from upper to lower direction, which are upper background, upper wall, lumen, lower wall, and lower background.

The graph cut energy function formulation is then given by:

$$E(L) = \sum_{p \in P} D(L_p) + \lambda \sum_{\{p,q\} \in N} V(L_p, L_p)$$

where P is the set of pixels; N are the neighboring pixels for pixel p in polar coordinates; and L denotes the class label. λ is the weight factor between the data term D and the smoothness term V. The data term D is given by:

$$D(L_p) = -\log(\Pr(L_p|I_p, d_p) + \varepsilon), V(L_p, L_q) = \begin{cases} \exp(-|I_p - I_q|/A) & L_p \neq L_q \\ 0 & L_p = L_q \end{cases}$$

where $\Pr(L_p|I_p, d_p)$ is the product of the pixel's conditional probabilities to belong to the lumen, wall, or background classes given its image intensity value I_p and distance from the lumen-wall boundary d_p. A is a normalization factor. We assume that these probabilities have Gaussian distribution $N(\mu_I^L, \sigma_I^L), N(\mu_d^L, \sigma_d^L)$. We use an iterative approach, where in each iteration we alternate between estimating the parameter of the Gaussian distributions and optimizing the energy of graph cut segmentation. We initialize the parameters of the Gaussian distribution using typical values for the wall and background and using the values at the positioned centerline seed points for the lumen.

After obtaining the segmentation results, we extract the contours of the wall and the lumen and then manually refine

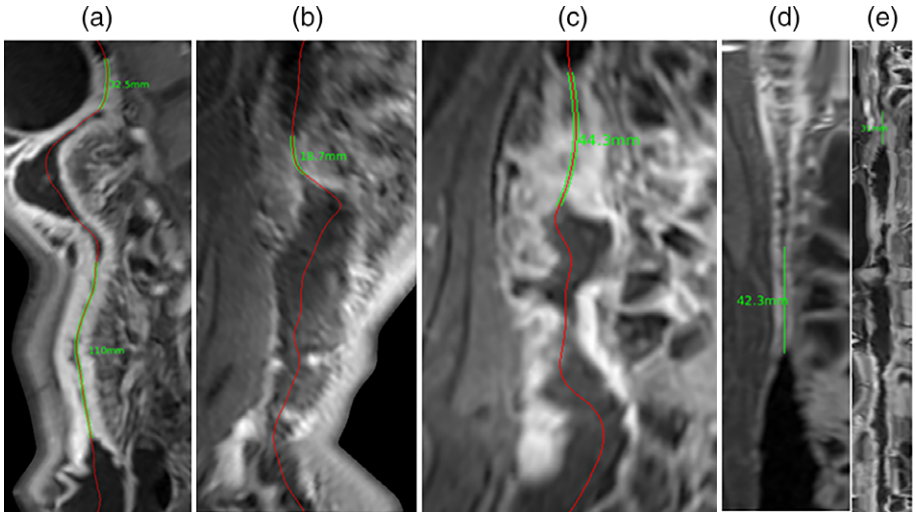

FIGURE 1: Demonstration of stretched (a–c) and straightened CPR views (d,e) of small bowel segments of five different patients with CD. Green curves demonstrate measurements of regions with narrowing (stricture). These views enable rapid evaluation of the diseased bowel segment and the luminal narrowing and/or wall thickening of the diseased bowel segment without the need to scroll through each plane to follow curved loops of the diseased bowel segment.

the results using the visual interface and the editing tool. The editing is performed on six discrete angles and with interpolation in between.

GENERATION OF VOLUMETRIC ANNOTATED DATA REPRESENTATION. We use the points on the oriented contours to construct a tetrahedral mesh. We then assign the voxels of each tetrahedron in the mesh with the proper lumen or wall annotation. The implementation of transferring from tetrahedral mesh into a volumetric representation is performed as follows:

Given a tetrahedron T, any point $p \in T$ divides it into four sub tetrahedrons.

The vector e of the point p with respect to vertex v can be expressed by:

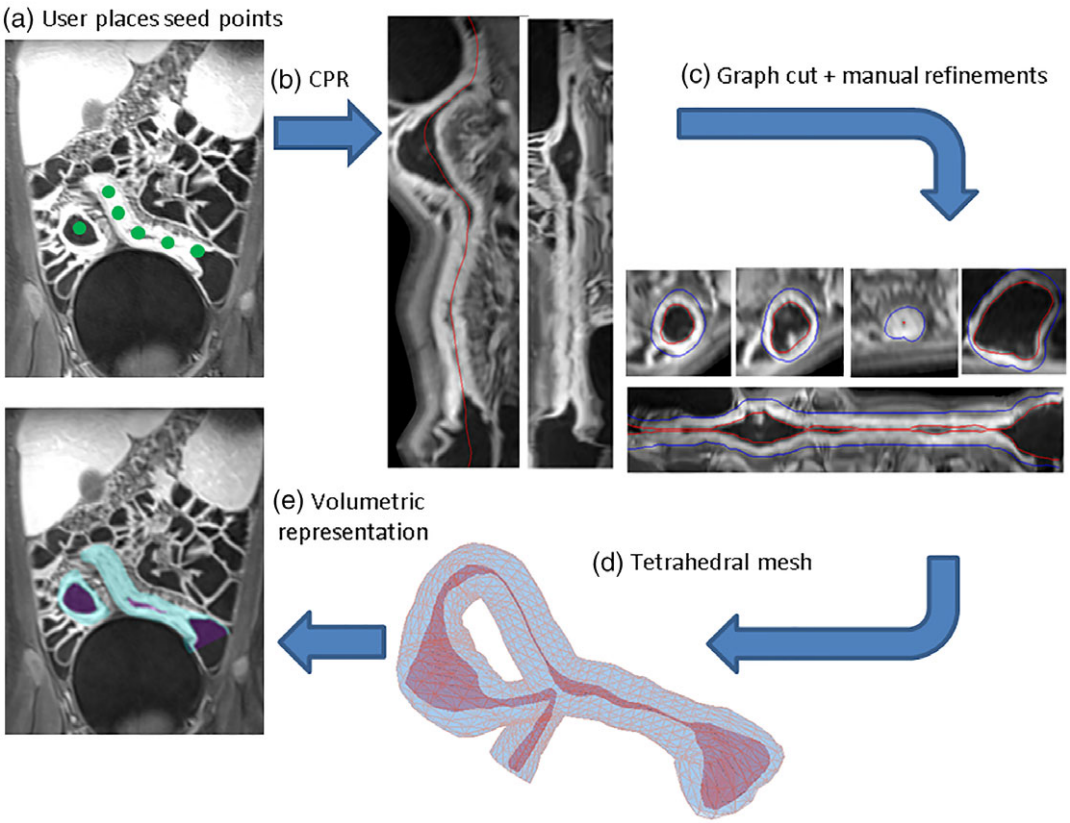

FIGURE 2: Generation of a labeled dataset of CD segments.

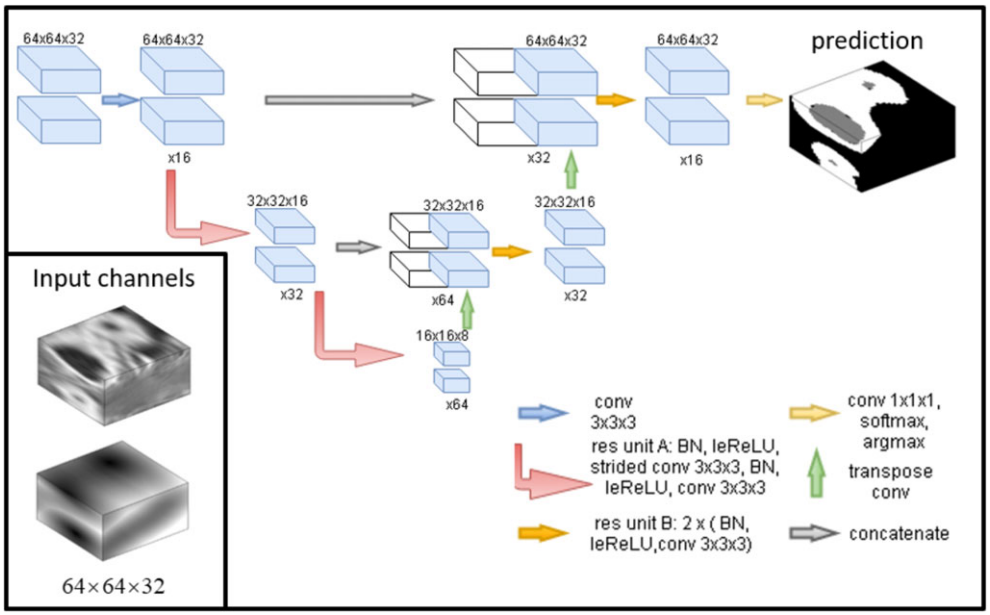

FIGURE 3: Left panel shows the network's two input patches (image intensity and distance prior) each of size 64 × 64 × 32 and the right panel shows the network architecture. For better demonstration, the two input channels are depicted one above the other, and the residual U-Net's concatenating channels are depicted alongside one another.

$$e = \alpha e_i + \beta e_j + \gamma e_k$$

Where the barycentric coordinates $(\alpha, \beta, \gamma) \in [0, 1]$ are the volume ratios between each subtetrahedron and tetrahedron T:

$$\alpha = \frac{\det(e, e_j, e_k)}{\det(e_i, e_j, e_k)} \beta = \frac{\det(e_i, e, e_k)}{\det(e_i, e_j, e_k)} \gamma = \frac{\det(e_i, e_j, e_k)}{\det(e_i, e_j, e_k)}$$

e_i, e_j, e_k are the tetrahedron edge vectors with respect to vertex v.

To ensure that the global orientation is consistent (ie, the Jacobians have equal signs), the ordering of the three vertices i, j, k when looking from vertex v should be either clockwise or counterclockwise for all tetrahedra.

To find the inner voxels surrounded by each tetrahedron, we take the grid pixels of the minimal box that bounds the tetrahedron and looked up the pixels whose barycentric coordinates apply:

$$\alpha, \beta, \gamma \geq 0 \; \alpha + \beta + \gamma \leq 1$$

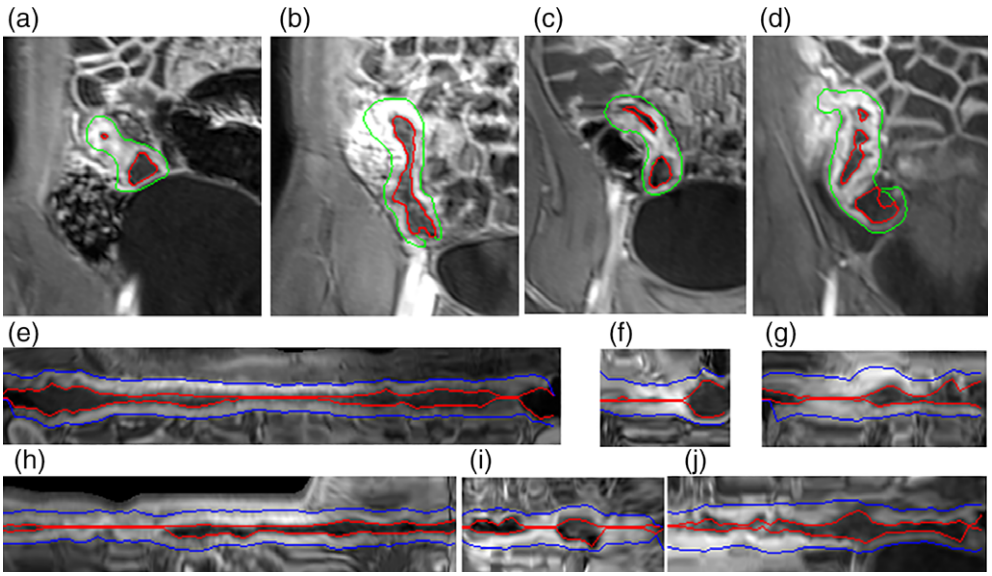

FIGURE 4: Segmentation results of the convolutional neural network algorithm of several different patients in coronal images (upper) and in straightened CPR views (lower).

Figure 2 demonstrates the annotation generation process.

CNN-Based Lumen and Wall Segmentation With Distance Map Channel Prior

Our motivation for using a 3D CNN segmentation algorithm is based on the observation that the highly variable bowel appearance and shape requires a supervised algorithm that can learn feature representations and a classifier from a large set of augmented training patches for solving this difficult problem. The purpose of the network is to segment 3D patches centered on seed points along the centerline into lumen, wall, and background classes. The obtained prediction scores of the 3D patches are then combined (by averaging the probabilities in overlapping pixels) to provide the final segmentation of the diseased bowel segment. We perform the segmentation in the original coronal image volumes instead of using CPR views to reduce the dependency of the segmentation performance on the quality of the initial centerline delineation. The segmentation of the small bowel is challenging because one diseased section of the wall can be adjacent to either part of the same diseased segment, or part of a distal healthy segment. In addition, the lumen and the mesentery might have similar intensities such that, from a patch perspective, it may be unclear whether a region is inside the lumen or between two walls. To overcome this ambiguity, we added a distance map prior as an additional input to our algorithm. Accordingly, the distance prior is computed as the shortest distance of each voxel from the interpolated centerline seed points positioned in the lumen.

Our CNN network, shown in Fig. 3, has a 3D fully connected U-Net architecture[15] with residual units.[16] The network has three contracting layers; three expanding layers; and a final convolution layer (with kernel size one) followed by softmax. Each residual layer has two sets of batch normalization, leaky ReLU activation, and convolution, as suggested previously.[16] Downsampling and upsampling of features is done using strided convolutions and transpose convolutions, respectively. The input to the network consists of two channel patches of size $64 \times 64 \times 32$ (the full image size after interpolation for generating isotropic pixel-size of 0.75 mm is $512 \times 432 \times 162$). The first channel patches were taken from the contrast-enhanced T_1-weighted MR images after resampling to isotropic resolution. Before cropping the patches, the images were normalized to have zero mean and a standard deviation equal to 1. The patches were centered on randomly selected lumen pixels. The rationale for this selection was to ensure the robustness of the segmentation to variability in the selection of lumen seed points.

We scale the distances to the range of [–1, 1] after truncating the max value to 32. We trained the network with a stochastic gradient descent with momentum of 0.9 and L2 regularization with lambda = 10^{-3}. To augment the training data, we added Gaussian noise, random rotations over the x-axis, random scaling of ±10%, and random flips in each of the three dimensions. Figure 3 illustrates the network's input patches and its architecture.

Experiments

An Institutional Review Board (IRB) approval waiving the requirement of consent was obtained prior to retrospective collection of data from clinically acquired images. We retrospectively searched for T_1-weighted VIBE scans of pediatric Crohn's disease patients with

TABLE 1. Performance of the Network in Segmenting the Small Bowel Lumen and Wall

	DSC[%] lumen	DSC[%] wall	DSC[%] background	Median BD[mm] lumen	Median BD[mm] wall	Average BD[mm] lumen	Average BD[mm] wall	Cross entropy
Single input channel	55 ± 25	60 ± 17	93 ± 4	0.83 ± 2.8	1.7 ± 4.0	1.6 ± 2.8	3.4 ± 4.0	0.34
Distance prior concatenated at the final layer	70 ± 19	75 ± 10	95 ± 4	0.83 ± 1.8	1.8 ± 3.1	1.2 ± 1.8	3.1 ± 3.1	0.22
Proposed method with distance channel prior	75 ± 18	81 ± 8	97 ± 2	0.82 ± 1.5	0.85 ± 2.4	1.0 ± 1.5	1.8 ± 2.4	0.13

DSC, Dice similarity coefficient, DB, distance boundary (between the CNN result and the label).

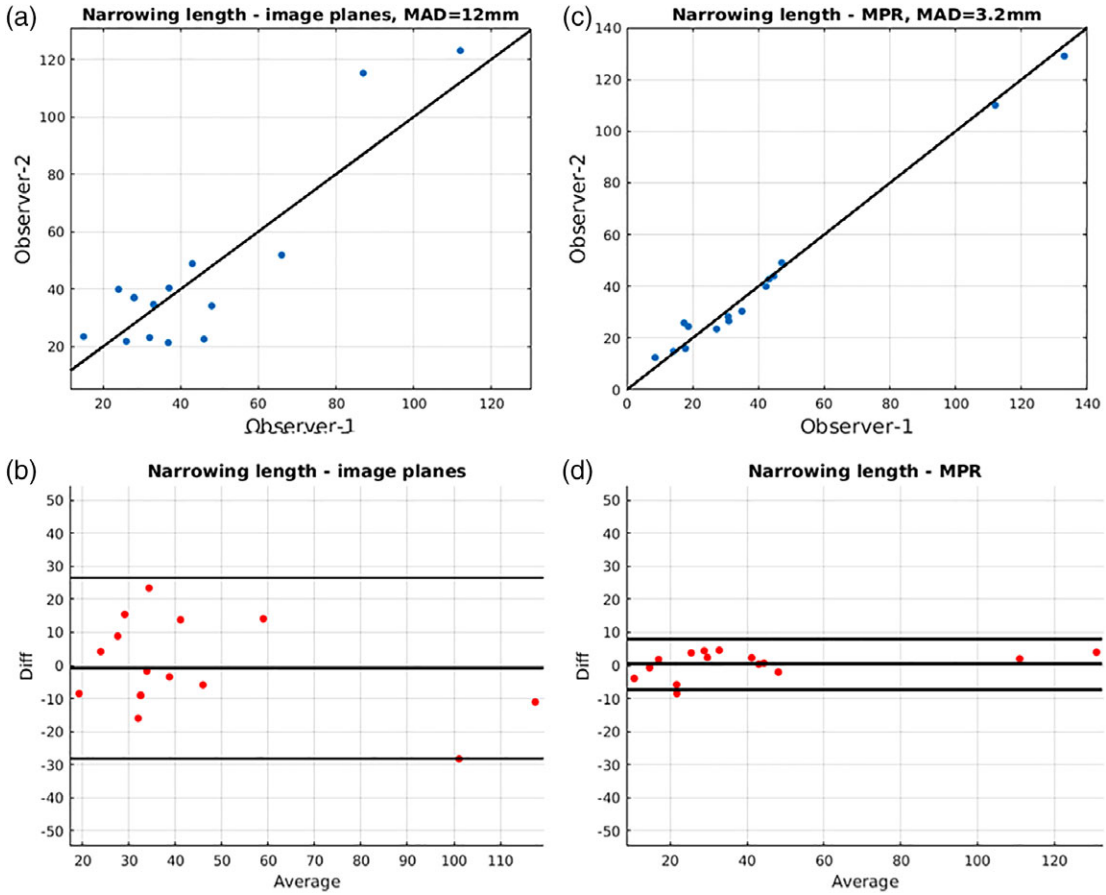

FIGURE 5: Comparison of stricture/luminal narrowing length measurements in CPR views vs. measurements in the original acquisition images. There was better accuracy and reproducibility of stricture/luminal narrowing length measurements in the CPR views. Mean Absolute difference (MAD) of 3.2 mm in CPR vs. 12 mm in the original images.

slice thickness lower than 2 mm that also have sufficient bowel distension and good image quality. All selected images were acquired using a T_1-weighted VIBE sequence in a 1.5T Siemens Avanto scanner (Erlangen, Germany) before and after contrast injection. We analyzed 23 pediatric patients with active (n = 17) and nonactive (n = 6) CD. Two abdominal radiologists, J.P.R. and M.K. with 20 + years of experience and who are specialized in CD MRI, evaluated all cases separately. In cases of disagreement between the radiologists, a third session was carried out to discuss each case to reach consensus.

The images were acquired in coronal planes with pixel size of about 0.75 × 0.75 × 2 mm. The acquisition protocol included sequential multiplanar MR images of the abdomen and pelvis both prior to and following the administration of intravenous contrast. Prior to the scan, the patients were prepped to increase bowel lumen distension (Polyethylene Glycol 3350, Bayer, Berlin, Germany) and reduce peristalsis (Glucagon).

To perform an evaluation of both the proposed markers extraction pipeline that includes manual editing and the CNN segmentation, we evaluated the method's ability to extract markers that can differentiate between different levels of disease on the entire dataset and separately evaluated the CNN segmentation performance after splitting the dataset into train and test sets.

CNN SEGMENTATION OF THE SMALL BOWEL LUMEN AND WALL. We generated a labeled dataset of the small bowel lumen and wall according to the above description. We divided the dataset into 15 and 8 cases from which we extract patches for training and testing the network, respectively. In total, we generated over 2.5 million augmented patches for training and several thousand patches for testing. All patches include a short tube of the disease small bowel in various directions, radiuses, and thicknesses. The training took about 8 days on a GPU (NVIDIA, GTX) with 8 MB memory using Tensorflow.[21]

CROHN'S MARKERS EXTRACTION PIPELINE. To evaluate the accuracy of measurement of length of strictures or regions with narrowing using CPR compared with measurement using original image planes, two observers marked the region on stretched or straightened CPR views and on the original planes using one or more line measurements on 15 segments with stricture or narrowing. The agreements between the observers' measurements on the CPR and the original images were calculated.

To test the ability of our method to extract CD activity markers, we used the segmentations (after manual refinement using our editing tool when needed) to calculate the wall thickness at the location of maximal luminal narrowing and median relative contrast enhancement in 22 active and six

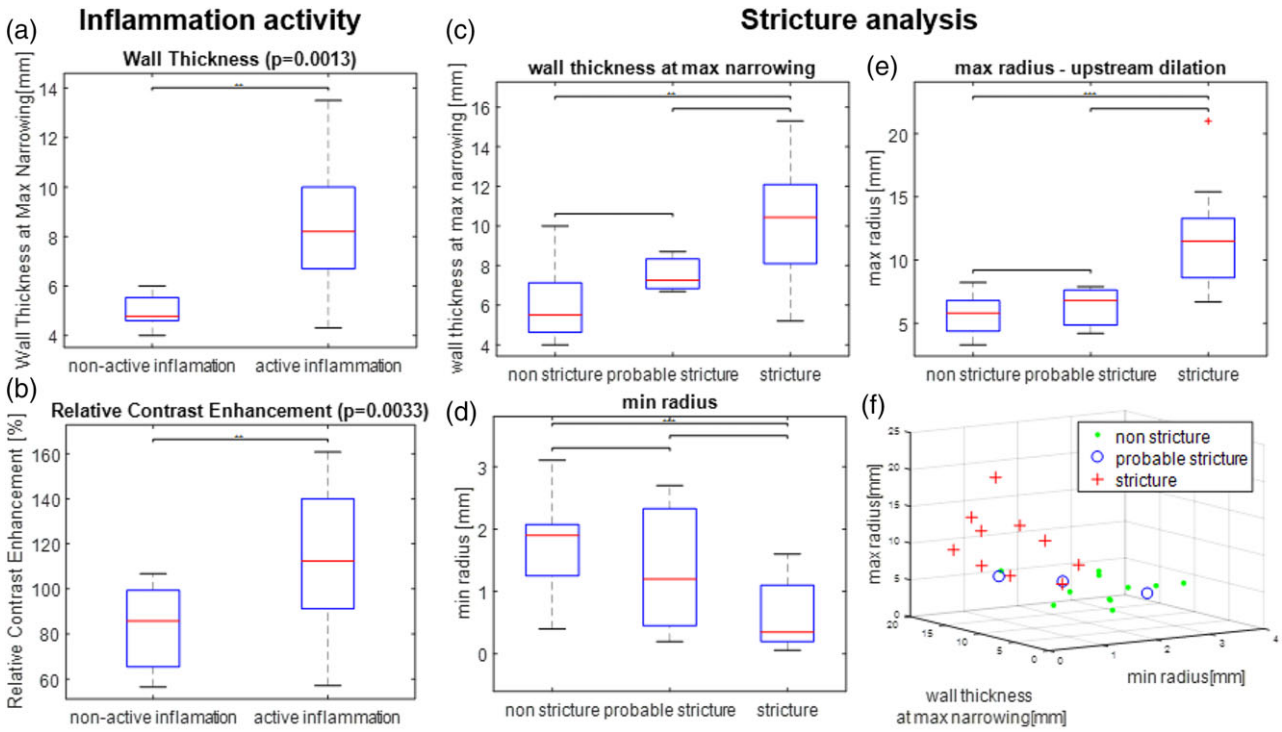

FIGURE 6: Performance of the extracted markers in differentiating between active and nonactive inflammation and between stricture, probable stricture, and nonstricture small bowel segments. Asterisks represent statistically significant discrimination ($P < 0.05$). The analysis included manual refinement.

nonactive disease segments. For analyzing stricture and luminal narrowing, we extracted three quantitative imaging markers: 1) the minimum radius as a marker of narrowing; 2) the wall thickness at the location of minimum radius, as a marker of active inflammation; and 3) the maximum radius as a marker of bowel dilation proximal to the stricture. We computed these three markers and compared their values in 21 segments without strictures, six segments with strictures, and three segments marked by the reporting radiologist to have a probable stricture.[1]

We designed an experiment to test the reproducibility of the method to generate the CPR views as follows. A user (Y.L.) with experience of 2 years in generating CPR views in cardiovascular images and with experience in MRE imaging of CD, used the proposed tool to extract markers twice from two different phases of multiphase postcontrast images from the same study. The two analyses were performed with at least 1-month time separation to ensure that the user had limited intellectual recall of the first analysis. Note that due to the motility of the bowel and the enlargement of the bladder, the two image volumes provide two different poses of the small bowel.

Statistical Analysis

To estimate our network's segmentation performance on the test set, we calculated the cross-entropy and the Dice similarity coefficient (DSC) for the lumen, wall, and background classes. In addition, we calculated the mean and median boundary distances (BD) between the CNN and manual delineations of the lumen-wall and wall-background boundary contours.

The capability of the extracted imaging markers to differentiate between different disease levels was determined using a *t*-test.

For the reproducibility test, we assessed the agreement between markers' measurements at different timepoints using the mean relative difference (MRD), Pearson correlation, and Bland–Altman analysis.

Results

Figure 4 demonstrates the results of the model's lumen and wall segmentation in the original coronal plane and after reformation of the segmentation results in straightened CPR views. Table 1 summarizes the performance of the proposed CNN architecture with distance prior in segmenting the small bowel lumen and wall. When integrating the distance prior into the proposed 3D Residual U-Net's architecture, the Dice coefficients increased from 55–75% for the lumen, and from 60–81% for the wall segment. The median distance between the automated and manually labeled contours reduced from 1.70 mm to 0.85 mm and from 1.6 mm to 1.0 mm for the lumen-wall and wall-background boundaries, respectively.

When comparing the level of agreement between two observers in measuring luminal narrowing length, there was a mean absolute difference of 12 vs. 3.2 mm when the

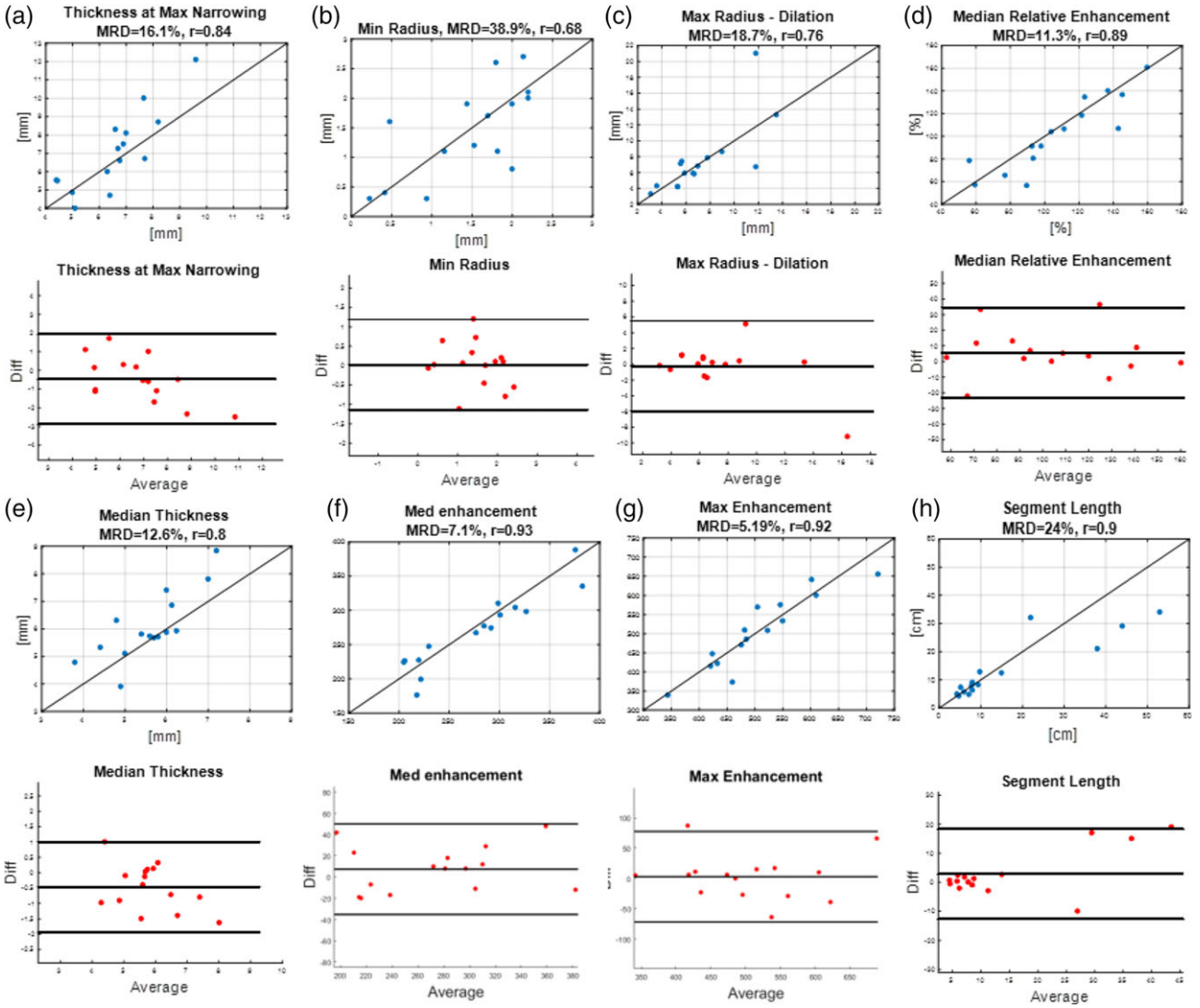

FIGURE 7: Estimated reproducibility of various CD image markers. Satisfactory reproducibility was found for median wall thickness, wall thickness at minimum radius, relative contrast enhancement, median enhancement, maximum enhancement, maximum radius, and length of abnormality for <20 cm segments. Moderate reproducibility was obtained for min radius and for length of abnormality for >20 cm segments.

measurement was performed on the original images compared with the CPR views, respectively (Fig. 5).

The wall thickness at the location of min radius (P = 0.0013) and the median value of relative contrast enhancement (P = 0.0033) could differentiate active and nonactive disease segments with statistical significance. The results are shown in Fig. 6.

The results showed that when analyzing markers to identify the presence of stricture, statistical significance was found between nonstricture segments and stricture segments when using each of the three markers. These results and combinations of markers are also shown in Fig. 6 (right panel). No statistical significance was found between segments with probable stricture and segments with strictures or without strictures. The results are demonstrated in Fig. 6.

The reproducibility of the extracted quantitative image markers are demonstrated in Fig. 7. The results are reported for image markers including median wall thickness, wall thickness at min radius, relative contrast enhancement, maximum radius (bowel dilation), median thickness, median contrast enhancement, maximum enhancement, and diseased segment length.

3D Surface Visualization of Crohn's Imaging Markers

We reconstructed surfaces from the segmentation contours and displayed the wall thickness and lumen narrowing as colormaps (Fig. 8).

Discussion

To provide optimal care for patients with pediatric CD, response to therapy and disease severity must be assessed as early as possible during the course of the disease. Moreover, a timely and accurate diagnosis has important prognostic

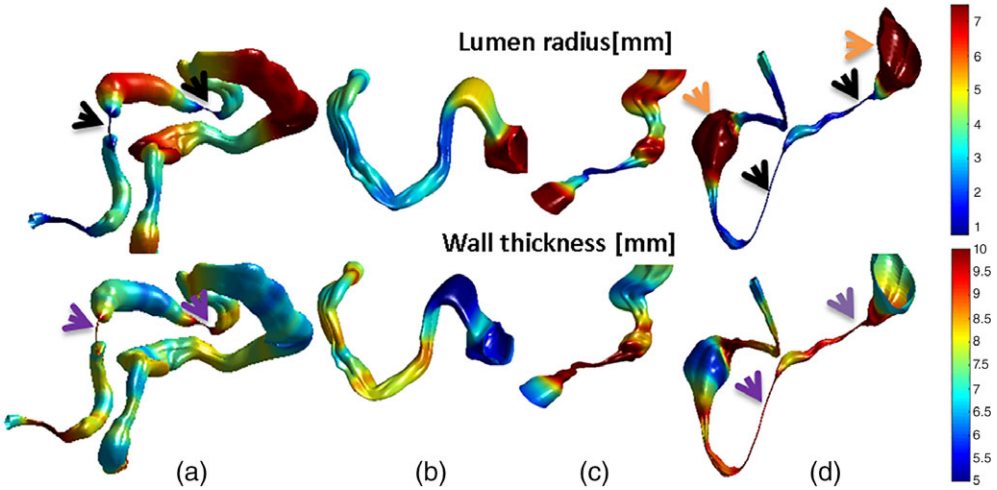

FIGURE 8: Surface rendering of the lumen boundary with colormaps indicating lumen radius [mm] (upper row) and wall thickness [mm] (lower row) obtained using the proposed method. This visualization demonstrates effectively the extent and severity of different regions along the diseased segment. Cases (a) and (d) have diseased areas with strictures that have a very narrow lumen (black arrows) and a very thickened bowel wall (magenta arrows) that may indicate surgical therapy. In case (d), there are locations with bowel dilations (orange arrows).

implications. The use of MRI for assessing pediatric CD has increased dramatically, especially as we strive to spare children the potentially harmful effects of radiation when imaged with computed tomography. Thickness and relative contrast enhancement of the wall, length of the inflamed bowel segment, and the extent of luminal narrowing are important imaging markers of disease activity.[2] However, due to the curved structure of the bowel, these features are often difficult to measure in the coronal or axial acquisition planes. It is also labor-intensive to extract these markers manually and therefore quantitative markers are not routinely used in the clinic. In addition, the lack of spatial alignment in follow-up scans makes it challenging to longitudinally compare the parameters for the same region.

Several studies have proposed semiautomatic methods for characterization of CD from MRI data.[10,11,22] However, the use of CPR views for assessment of CD has not been proposed due to limitations like motion artifacts, highly deformable shape of the bowel, and poor bowel distention. These factors limited the quality of acquired images in a single breath-hold. Despite these difficulties, we generated CPR views for about two-thirds of patients who were imaged with proper luminal distension and without major motion artifacts limiting image quality. The CPR platform enables improved visualization of the lumen narrowing and measurement of disease markers such as diseased segment length, wall thickness, and stenosis length. In addition, we used it to both generate a labeled dataset for training CNN-based segmentation of the bowel wall and as a platform where editing tools can be quickly applied to fine-tune the results.

Our CNN-based segmentation could successfully segment the bowel lumen and the wall. The performance when adding the distance map as an additional channel was superior to that seen when integrating the distance prior at the final layer—an observation that implies that integrating spatial information to the learned image filters improves overall performance. Such spatial informative channels may improve the performance in other image segmentation applications as well. We observed that there were several locations where the algorithm delineated the boundaries more accurately than the labeled data. For cases that require manual refinement, our proposed editing software enables efficient and quick manual editing of the segmentations on CPR views before computing the disease markers.

When compared with prior work for small bowel segmentation (Table 2), our work is the only method to report segmentation performance in segmenting the lumen, wall, and background classes. Some works segment regions affected by CD without separation between the lumen and wall. These works cannot extract measurement of wall thickness or lumen narrowing. Other works perform semiautomated segmentation of the wall for evaluating its thickness, but do not provide any segmentation performance values.[11]

With regard to stricture length measurements, better agreement was obtained when the measurement was done on the CPR image versus a measurement from the original images.

The differences between quantitative imaging markers of disease that were computed by the proposed method in segments with active and segments with nonactive inflammation, and in segments with strictures and segments without strictures, were statistically significant. This highlights the potential of the proposed tool in both analyzing bowel wall thickness and tissue enhancement for assessment of response to therapy as well as assessing luminal narrowing and dilation in CD for optimizing surgical decisions.

The estimated reproducibility of median wall thickness, wall thickness at minimum radius, relative contrast enhancement, median enhancement, maximum enhancement, and

TABLE 2. Comparison to CD Small Bowel Segmentation Prior Work

Method	Provide the entire disease segment?	Can be used to extract disease markers?	Lumen DSC	Wall DSC	Background DSC	Lumen+wall vs. background DSC
SL(3)	No	No	N/A	N/A	N/A	86.5 ± 2.3%
WSS (9)	No	No	N/A	N/A	N/A	75.3%
RF[SPIE2013]	No	No	N/A	N/A	N/A	91.9 ± 1.9
SS-AL (6)	No	No	N/A	N/A	N/A	92.1%
AS(4)	No	No	N/A	N/A	N/A	90 ± 4%
AL (5)	No	No	N/A	N/A	N/A	92.7%
CNN (ours)	Yes	Yes	75 ± 18%	81 ± 8%	97 ± 2%	No Need

All prior works with reported segmentation performance segment the wall and lumen together from their background instead of each compartment alone. These works provide small tissue segments with CD instead of tube structure and therefore cannot extract the wall thickness or lumen narrowing. Other works[11,24] for segmenting the small bowel wall and for extracting its thickness do not report any segmentation performances.

maximum radius were good. The estimated reproducibility measure of the abnormal segment length was good for segments 20 cm or less, and moderate for segments longer than 20 cm. This might be associated with the difficulty to determine the start or end point of the abnormality in long segments. The estimated reproducibility measure of the minimum radius was moderate. This may be due to limited resolution, resulting in decreased accuracy of the measurement.

Our study design includes several limitations. First, our references were based on consensus of two independent expert radiologists and did not contain any histological validation. Such validation may not be considered as the absolute reference standard. However, for our preliminary feasibility study we assume that it is sufficient for getting a proof of concept for our method. Second, our study was performed retrospectively, which may introduce some level of bias. Third, we analyzed only 23 cases that were acquired with the required resolution (ie, pixel size <2 mm in each direction) and that also have sufficient image quality for the proposed analysis. This limitation is associated with the difficulty in placing seed points along the centerline in images with significant motion artifacts, poor bowel distension, or severe disease where the lumen path is barely visible. With the development of faster and motion-robust MRI techniques, we expect that most patients will have good-quality images and will benefit from the proposed image analysis technique.

Future studies will focus on other disease imaging markers such as diffusion-weighted MRI. This additional information can be jointly or separately extracted after registration of the images acquired in the same imaging session.[23]

In conclusion, we propose a novel method for analyzing diseased small bowel segments and for extracting quantitative imaging markers of disease activity in T_1-weighted, contrast-enhanced MR images of pediatric CD patients. Our method involves generating CPR images of the small bowel and enables rapid segmentation of the small bowel lumen and wall using a 3D residual CNN with a distance prior. To the best of our knowledge, this is the first evaluated method for segmenting the diseased small bowel that includes the lumen, wall, and background classes. Such analysis facilitates the computation of imaging markers for estimating disease severity and response to therapy. We anticipate that the proposed method may promote clinical utilization of these imaging markers for characterization and assessment of pediatric CD.

Acknowledgment

This investigation was supported in part by NIH grants R01 NS079788, R01 EB019483, R01 DK100404, R44 MH086984, IDDRC U54 HD090255, and by a research grant from the Boston Children's Hospital Translational Research Program.

Contract grant sponsor: Crohn's and Colitis Foundation of America's Career Development Award; Contract grant sponsor: AGA-Boston Scientific Technology & Innovation Pilot Research Award; Contract grant sponsor: National Institute of Diabetes and Digestive and Kidney Diseases (NIDDK) of the NIH; Contract grant number: R01DK100404.

References

1. Bruining DH, Zimmermann EM, Loftus EV, Sandborn WJ, Sauer CG, Strong SA. Consensus recommendations for evaluation, interpretation, and utilization of computed tomography and magnetic resonance

enterography in patients with small bowel Crohn's disease. Gastroenterology 2018;154:1172–1194.

2. Rimola J, Rodríguez S, García-Bosch O, et al. Magnetic resonance for assessment of disease activity and severity in ileocolonic Crohn's disease. Gut 2009;58:1113–1120.
3. Mahapatra D, Schueffler P, Tielbeek JA, Buhmann JM, Vos FM, eds. A supervised learning based approach to detect crohn's disease in abdominal MR volumes. *International MICCAI Workshop on Computational and Clinical Challenges in Abdominal Imaging*; 2012: Berlin, Springer.
4. Mahapatra D, Schuffler PJ, Tielbeek JA, et al. Automatic detection and segmentation of Crohn's disease tissues from abdominal MRI. IEEE Trans Med Imaging 2013;32:2332–2347.
5. Mahapatra D, Schüffler PJ, Tielbeek JA, et al., eds. Active learning based segmentation of Crohn's disease using principles of visual saliency. Biomedical Imaging (ISBI), 2014 I.E. 11th International Symposium on; 2014: IEEE.
6. Mahapatra D, Schüffler PJ, Tielbeek JA, Vos FM, Buhmann JM, eds. Semi-supervised and active learning for automatic segmentation of crohn's disease. International Conference on Medical Image Computing and Computer-Assisted Intervention; 2013: Berlin, Springer.
7. Mahapatra D, Schüffler PJ, Tielbeek JA, Vos FM, Buhmann JM, eds. Crohn's disease tissue segmentation from abdominal MRI using semantic information and graph cuts. Biomedical Imaging (ISBI), 2013 I.E. 10th International Symposium on; 2013: IEEE.
8. Mahapatra D, Schüffler PJ, Tielbeek JA, Vos FM, Buhmann JM, eds. Localizing and segmenting Crohn's disease affected regions in abdominal MRI using novel context features. Medical Imaging 2013: Image Processing; 2013: International Society for Optics and Photonics.
9. Mahapatra D, Vezhnevets A, Schüffler PJ, Tielbeek JA, Vos FM, Buhmann JM, eds. Weakly supervised semantic segmentation of Crohn's disease tissues from abdominal MRI. Biomedical Imaging (ISBI), 2013 I.E. 10th International Symposium on; 2013: IEEE.
10. Naziroglu RE, Puylaert CA, Tielbeek JA, et al. Semi-automatic bowel wall thickness measurements on MR enterography in patients with Crohn's disease. The British journal of radiology. 2017;90:20160654.
11. Vos FM, Tielbeek JA, Naziroglu RE, et al., eds. Computational modeling for assessment of IBD: to be or not to be? Engineering in Medicine and Biology Society (EMBC), 2012 Annual International Conference of the IEEE; 2012: IEEE.
12. Kanitsar A, Fleischmann D, Wegenkittl R, Felkel P, Gröller ME, eds. CPR: curved planar reformation. Proceedings of the Conference on Visualization '02; 2002: IEEE Computer Society.
13. Litjens G, Kooi T, Bejnordi BE, et al. A survey on deep learning in medical image analysis. Med Image Anal 2017;42:60–88.
14. Shen D, Wu G, Suk H-I. Deep learning in medical image analysis. Annu Rev Biomed Eng 2017;19:221–248.
15. Ronneberger O, Fischer P, Brox T, eds. U-net: Convolutional networks for biomedical image segmentation. International Conference on Medical image computing and computer-assisted intervention; 2015: Berlin, Springer.
16. He K, Zhang X, Ren S, Sun J, eds. Identity mappings in deep residual networks. European Conference on Computer Vision; 2016: Berlin, Springer.
17. Willmore TJ. An introduction to differential geometry: Courier Corporation; 2013.
18. Weatherburn CE. *Differential geometry of three dimensions*. Cambridge, UK: Cambridge University Press; 2016.
19. Orfanidis S. Introduction to signal processing: Pearson Education; 2010.
20. Boykov Y, Funka-Lea G. Graph cuts and efficient ND image segmentation. Int J Comput Vis 2006;70:109–131.
21. Pawlowski N, Ktena SI, Lee MC, et al. Dltk: State of the art reference implementations for deep learning on medical images. arXiv preprint arXiv:171106853. 2017.
22. Hampshire T, Menys A, Jaffer A, et al. A probabilistic method for estimation of bowel wall thickness in MR colonography. PLoS One 2017;12: e0168317.
23. Kurugol S, Freiman M, Afacan O, et al. Motion-robust parameter estimation in abdominal diffusion-weighted MRI by simultaneous image registration and model estimation. Med Image Anal 2017;39:124–132.
24. Schüffler PJ, Mahapatra D, Naziroglu R, et al., eds. Semi-automatic Crohn's Disease Severity Estimation on MR Imaging. International MICCAI Workshop on Computational and Clinical Challenges in Abdominal Imaging; 2014: Berlin, Springer.